



Contents lists available at ScienceDirect



Catalysis Today

journal homepage: www.elsevier.com/locate/cattod

WO_x modified Cu/Al₂O₃ as a high-performance catalyst for the hydrogenolysis of glucose to 1,2-propanediol

Chengwei Liu^{a,c}, Chenghua Zhang^{a,b,*}, Shunli Hao^b, Sikai Sun^b, Kangkai Liu^b, Jian Xu^b, Yulei Zhu^{a,b}, Yongwang Li^{a,b}

^a State Key Laboratory of Coal Conversion, Institute of Coal Chemistry, Chinese Academy of Sciences, Taiyuan 030001, PR China

^b National Energy Center for Coal to Liquids, Synfuels CHINA Co., Ltd., Huairou District, Beijing, 101400, PR China

^c University of Chinese Academy of Sciences, Beijing 100049, PR China

ARTICLE INFO

Article history:

Received 12 May 2015

Received in revised form 27 June 2015

Accepted 29 June 2015

Available online xxx

Keywords:

WO_x

Cu-WO_x/Al₂O₃

Glucose

Hydrogenolysis

1,2-Propanediol

ABSTRACT

Glucose is one of the most important platform molecules of biomass in nature. The selective hydrogenolysis of glucose to 1,2-PDO is still a challenge. However, the hydrogenolysis of fructose has higher activity and selectivity to 1,2-PDO. Therefore, a series of Cu-WO_x/Al₂O₃ catalysts with high activity for glucose isomerization to fructose and fructose hydrogenolysis to 1,2-PDO were designed for glucose hydrogenolysis to 1,2-PDO. The W surface density was controlled as low as 0.8 W/nm². The low W surface density could make the WO_x species present as isolated WO₄ structure, which could only provide more Lewis acid sites. As a result, the isolated WO₄ species could form a complex with glucose and then promote the isomerization of glucose to fructose. The isolated WO₄ species also have coverage, dispersion, and electronic effects on copper sites, resulting more stable copper sites and proper amount of hydrogenation sites on Cu-WO_x/Al₂O₃ surface. The correlations between the ratio of Lewis acid amount to Cu surface area and the selectivity of 1,2-PDO suggest that the hydrogenolysis of glucose to 1,2-PDO follows the bifunctional reaction route which contains the reactions on Lewis acid and metal sites. Furthermore, the highest 1,2-PDO selectivity of 55.4% was obtained on Cu-WO_x(0.8)/Al₂O₃.

© 2015 Elsevier B.V. All rights reserved.

1. Introduction

Increasing interests have been stimulated in developing novel chemical processes based on renewable biomass materials for producing energy and chemicals in view of the depletion of fossil resources and ongoing climate change [1–4]. Among biomass based feedstocks, glucose, as the monomer of cellulose, is an attractive platform chemical which can be efficiently converted into various chemicals, fuels, foods, medicines [5]. Furthermore, it is the most abundant monosaccharide and readily available from the hydrolysis of cellulose by mineral acids [5]. Therefore, the catalytic transformation of glucose is of great importance for biomass utilization. On this respect, the chemical routes for monosaccharide reactions such as oxidation, dehydration, esterification, hydrogenation, and hydrogenolysis have been reported on many

reviews [2,6–9]. Many value-added chemicals and biofuels such as 5-hydroxymethylfufural (HMF), 2,5-dimethylfuran, levulinic acid, γ -valerolactone, gluconic acid, pentanoic acid ester, and various polyols have been studied extensively recently [10]. Especially, hydrogenolysis, which results in the cleavage of C–C and C–O bonds by hydrogen, can produce valuable platform chemicals such as propanediol (PDO) and ethylene glycol (EG) that are already integrated in today's value chain. Furthermore, the hydrogenolysis of glucose in aqueous solution can avoid the fatal disadvantages in biomass conversion, such as the feedstock transportation, batch reaction, coking, organic solution, environment pollution, etc. All these merits make glucose an ideal feedstock in future large-scale biorefining. Therefore, the process of glucose hydrogenolysis in aqueous solution is respected to bear the potential to bridge currently available technologies and the future biomass-based refinery concepts [2].

In the earliest stage of the hydrogenolysis reaction of glucose and its derived-polyols sorbitol, glycerol was considered as the most desirable product. However, with the surplus of glycerol from biodiesel production, the importance of polyols-related value-added chemicals has shifted towards 1,2-propanediol (1,2-PDO) and ethylene glycol (EG). Furthermore, 1,2-PDO is an industrially

* Corresponding author at: State Key Laboratory of Coal Conversion, Institute of Coal Chemistry, Chinese Academy of Sciences, Taiyuan 030001, PR China. Tel.: +86 010 69667802.

E-mail addresses: zhangchh@sxicc.ac.cn (C. Zhang), [\(Y. Zhu\)](mailto:zhuyulei@sxicc.ac.cn).

important chemical and is extensively used in the production of polyester resins, pharmaceuticals, tobacco humectants, paints, cosmetics and antifreeze [11]. It is currently produced at an industrial scale using petroleum based propylene as the carbon feedstock. The hydrogenolysis of biomass-derived glucose to 1,2-PDO provides a sustainable and economic route instead of the oxidation of fossil fuel-derived propylene.

Cu, Ni, Ru based catalysts together with base additives such as CaO were often used for the hydrogenolysis of glucose and sorbitol, and a mixture of lower polyols such as glycerol, EG, and 1,2-PDO was mainly obtained. For example, Ye [12] reported a Ce-promoted Ni/Al₂O₃ catalyst for aqueous-phase hydrogenolysis of sorbitol to glycols. At 513 K and 7.0 MPa, above 90% of sorbitol conversion and 55–60% of glycol selectivities were obtained. Chen [13] found that the Ni/MgO catalyst with Ni/MgO ratio of 3:7 exhibited the best performance for sorbitol hydrogenolysis at 473 K and 4 MPa H₂, with 67.8% conversion and 80.8% total selectivity of EG, 1,2-PDO and glycerol. Banu [14] studied the conversion of sorbitol on Ni-NaY and Pt-NaY catalysts. They found that 1,2-PDO was the major product on Ni-NaY and glycerol was the main product on Pt-NaY. Meanwhile, the highest 1,2-PDO selectivity of 72% was achieved at 59% sorbitol conversion on Ni(6%)-Pt(1%)/NaY at 493 K and 6 MPa. A copper-chromium catalyst was more selective for 1,2-PDO. As reported by Zartman [15], a 60% yield of 1,2-PDO was obtained from glucose hydrogenolysis in supercritical ethanol. The CuCr catalyst was also reported to be efficient for the hydrogenolysis of cellulose to 1,2-PDO, with the yield of 42.6% [16]. Apparently, the study still encounters many problems such as poor activities and selectivities, harsh condition, and environmental pollution. Moreover, safe, efficient and economic catalysts are the key factor for the selective conversion of glucose to 1,2-PDO in aqueous solution.

It is well known that the hydrogenolysis of saccharides and polyols can be performed through a bifunctional reaction pathway that involves three primary reactions, C–O bond cleavage on acid sites, C–C bond cleavage and C=O/C=C bond hydrogenation on metal sites [17–19]. Furthermore, retro-aldol condensation is the key C–C bond cleavage reaction and occurs on metal sites [17]. However, it is well known that the retro-aldol condensation of glucose mainly produces C₂ and C₄ polyols, and the conversion of glucose to C₃ polyols includes two steps: the isomerization of glucose to fructose, which can be promoted by Lewis acid; the retro-aldol condensation of fructose to dihydroxyacetone and glyceraldehyde [20,21]. Therefore, based on the understanding of the reaction pathway, an efficient bifunctional catalyst with high activity for glucose isomerization, fructose retro-aldol condensation, dehydration and hydrogenation is required for the selective conversion of glucose to 1,2-PDO. Among the catalysts, Ni and Ru catalysts were frequently used for the hydrogenolysis of sugars and sugar alcohols due to their high activity for C–C bond cleavage. However, excessive C–C bond scission often happened, and large amount of unwanted products such as methane were formed [22]. It is known that copper catalyst has high activity for C–O bond cleavage and low activity for C–C bond cleavage. Such properties of copper based catalysts are suitable for the hydrogenolysis of glucose to glycols [22]. Moreover, the application of cheap metal can improve the economy of the hydrogenolysis route, which is one of the main challenges of the transformation process of renewable feedstocks [2]. As for the acid sites, alumina is a typical industrial support with large amount of acid sites on the surface. Furthermore, many studies have also been performed on the development of acid sites on tungsten oxide supported on alumina catalyst as a function of W surface density [23,24]. The studies turned out that the acid amount and acid species were easily tuned by changing the surface density of W. Furthermore, due to the strong interaction between the oxides, the WO_x phase is molecularly dispersed as a two-dimensional metal oxide overlayer on a high surface area support oxide with a high

stability [24]. The ratio of C–C/C–O bond cleavage can be tuned by modulating the concentration of acid to metal sites. A good balance between the two functions is very important to obtain a high yield of target polyols. Therefore, a non-noble Cu-WO_x/Al₂O₃ catalyst with different ratios of acid to metal sites by changing the density of W was designed. Cu/Al₂O₃ with proper activity for C–C/C–O bond cleavage and C=O bond hydrogenation showed a high activity for the hydrogenolysis of fructose to 1,2-PDO, and high dispersed WO_x species have a high selectivity for the isomerization of glucose to fructose. The synergy effect of the catalytic active site promotes glucose conversion and 1,2-PDO selectivity. This work focuses on the effect of W on the properties and catalytic performance of the Cu-WO_x/Al₂O₃ catalysts.

2. Experiment

2.1. Catalyst preparation

Cu/Al₂O₃ and WO_x modified Cu/Al₂O₃ catalysts (denoted as Cu-WO_x/Al₂O₃) with different WO_x weight loadings in the range of 1–7 wt% were prepared by a stepwise impregnation method. Firstly, γ-Al₂O₃ (purchased from Sinopharm Chemical Reagent Co., Ltd, China) was impregnated for 12 h with a certain amount of (NH₄)₆W₇O₂₄·6H₂O (Sinopharm Chemical Reagent Co., Ltd, China) aqueous solution. The impregnated sample was dried at 120 °C overnight. Afterwards, they were calcined at 600 °C for 4 h. The obtained sample was then impregnated for 12 h with an aqueous solution of Cu(NO₃)₂·3H₂O (Sinopharm Chemical Reagent Co., Ltd, China). After impregnation, the sample was dried at 120 °C overnight, followed by calcined at 350 °C for 4 h. The catalysts were labeled as Cu-WO_x(y)/Al₂O₃, in which y stands for the surface density of W (atoms/nm²). The Cu/Al₂O₃ catalyst was prepared using the stepwise impregnation method mentioned above.

2.2. Catalyst characterization

ICP optical emission spectroscopy (Optima2100DV, PerkinElmer) was performed to determine the chemical compositions of calcined catalysts.

BET surface areas were measured on a micromeritics ASAP 2420 instrument. All the samples were degassed at 110 °C for 1 h and 350 °C for 8 h prior to the measurement.

The surface areas of copper were calculated using N₂O chemisorption method performed based on the assuming spherical shape of the copper metal particles and 1.4 × 10¹⁹ copper atoms/m² [25,26]. Before the measurements, 200 mg sample was reduced by flowing H₂ at 250 °C for 2 h, followed by purging with He for 1 h. After cooled down to 50 °C, the sample was flushed with 10 vol.% N₂O/N₂ (50 mL/min) flow for 30 min. Then changed the gas flow to Ar (50 mL/min) and held for 30 min to clean the catalyst surface, finally the H₂-TPR was recorded with the 10 vol% H₂/Ar flow.

Powder X-ray diffraction (XRD) patterns were recorded on a D2/max-RA X-ray diffractometer (Bruker, Germany), with Cu-Kα radiation operated at 30 KV and 10 mA. The 2θ angle was scanned in the range of 10–80°.

H₂-TPR experiments were carried out on the Auto Chem II 2920 equipment (Micromeritics, USA) with a TCD detector. The sample (200 mg) was loaded in a quartz reactor and flushed with a 10 vol.% H₂/Ar flow at 50 °C. Then an isopropyl alcohol gel (−88 °C) cooled trap was added to condense the water vapor. The hydrogen consumption was monitored from 50 °C to 600 °C using a heating rate of 10 °C/min.

Raman spectra were recorded on a LabRAM HR800 System equipped with a CCD detector at room temperature. The 532 nm of the air-cooled frequency-doubled Nd-Yag laser was employed as the exciting source with a power of 30 MW.

UV-vis DRS spectra were collected on an Agilent cary 5000 UV-vis spectrometer with BaSO₄ as a reference. The calcined catalysts were measured in the 200–800 nm regions.

NH₃ temperature-programmed desorption (NH₃-TPD) measurements were performed on an Auto Chem II 2920 equipment (Micromeritics, USA). Prior to the test, 200 mg catalyst was reduced in a stream of pure H₂ at 250 °C for 2 h. Subsequently, the gas flow was changed to helium at 250 °C and then purged for 60 min to clean the surface. After cooling to 100 °C in the helium flow, the sample was adsorbed with NH₃ until saturation, then flushed with helium to remove the physical adsorption for 1 h. The NH₃ desorption pattern was recorded from 100 °C to 800 °C at a heating rate of 10 °C/min.

CO-FTIR spectra were collected using an infrared spectrometer (VERTEX70, Bruker, Germany), equipped with KBr optics which works at the liquid nitrogen environment. To realize the *in situ* measurement for the adsorption of CO, the infrared cell equipped with ZnSe windows was connected to a gas-feed system with a set of stainless steel gas lines. The catalysts were reduced *in situ* at 250 °C for 2 h in H₂ flow (20 mL/min), followed by flushing the sample with helium for 1 h at 250 °C. Then the CO-FTIR spectra were recorded after cooling to 30 °C in helium flow.

The Py-FTIR spectra were obtained on a VERTEX 70 Bruker FT-IR spectrometer. All the samples were reduced at 250 °C in H₂ for 2 h and then degassed to a pressure of 10⁻² MPa at 350 °C for 1 h. Adsorption of pyridine was carried out after cooling down to 30 °C. The Py-IR spectra were measured at 30 °C and 350 °C after evacuation for 30 min.

X-ray photoelectron spectroscopy (XPS) was performed on a Thermal XPS ESCALAB 250Xi spectrometer with Al K α radiation (1486.6 eV) and a multichannel detector. The obtained binding energies were calibrated using the C 1s peak at 284.6 eV as the reference. The experiment error reported in this study is within 0.1 eV. For the *in situ* reduction process, the sample was reduced at 250 °C for 2 h with a ramp of 1 °C/min.

2.3. Catalytic reaction process

Hydrogenolysis of glucose was performed in a vertical fixed-bed reactor (i.d. 12 mm, length 600 mm) with a cold trap. Prior to the test, 2.0 g catalyst (20–40 mesh) was loaded at the isothermal zone and *in situ* reduced at 250 °C for 2 h in hydrogen (100 mL/min). After reduction, a 5 wt% aqueous glucose solution was pumped into the reactor, and mixed with H₂ co-feeding. The liquid products were collected in a gas–liquid separator immersed in an ice–water trap. Typical reaction conditions were as follows: 4 MPa H₂ (45 mL/min), 5 wt% aqueous glucose solution, aqueous glucose solution flow rates were set as 24, 19.2, and 14.4 mL/h, which can be shown as 0.6, 0.48, and 0.36 h⁻¹ in WHSV (weight hourly space velocity).

The liquid products collected in the cold trap were analyzed offline by an HPLC equipped with a RID detector. The tail gas products were analyzed by online gas chromatograph (GC) (models 6890N and 4890D; Agilent). The conversion of glucose and the selectivity of products were calculated based on the total carbon according to the following equations:

$$\text{Conversion (\%)} = 100 - \frac{\text{carbon mol of reactant after reaction}}{\text{carbon mol of reactant in feedstock}} \times 100$$

$$\text{Selectivity (\%)} = \frac{(m_{\text{product}}/M_{\text{product}}) \times N_{\text{carbon numbers in product}}}{(m_{\text{glucose in feedback}} - m_{\text{glucose in products}})/M_{\text{glucose}}} \times 100$$

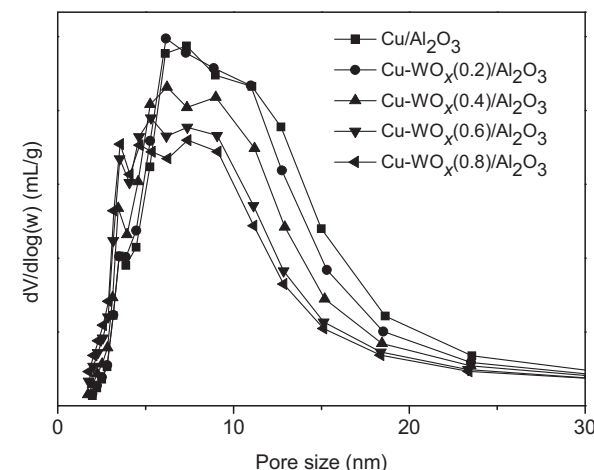


Fig. 1. The pore size distribution of calcined Cu-WO_x/Al₂O₃ catalysts.

where m : mass, M : relative molecular weight, N : carbon numbers in product.

More details about the analysis methods are in Supporting Information.

3. Results

3.1. Physicochemical properties of catalysts

The results of physicochemical properties of Cu-WO_x/Al₂O₃ catalysts are showed in Table 1. The copper loadings show little difference for different catalysts. The surface density of W species (W/nm²) was calculated from Eq. (1) [27,28]. The density of W increased with the designed amount. The highest W density was only 0.8 W/nm², which was much lower than the theoretical γ -Al₂O₃ monolayer coverage (7 W/nm²) [29,30]. The specific surface area and the pore structure of Cu-WO_x/Al₂O₃ catalysts are shown in Table 1 and Fig. 1. The BET surface area increased obviously with the increasing W density from 175.6 m²/g of Cu/Al₂O₃ to 218.7 m²/g of Cu-WO_x(0.8)/Al₂O₃. Both the pore volume and the pore size decreased slightly with increasing W density. Fig. 1 showed the pore size distribution of Cu-WO_x/Al₂O₃ catalysts. All the catalysts presented broad peaks centered at about 6.3 nm and a narrow peak centered at about 3.6 nm. The intensity of the peak at about 6.3 nm decreased while that of the peak at about 3.6 nm increased with increasing W density, indicating the penetration of WO_x into large pores to form pores of relatively small diameter. The metal dispersion is considered to be important parameter which strongly influences the catalytic performance. As shown in Table 1, the surface copper area decreased from 9.6 m²/gCat on Cu/Al₂O₃ to 6.0 m²/gCat on Cu-WO_x(0.8)/Al₂O₃.

$$\rho_W = \frac{[\text{WO}_3 \text{ loading (wt\%}/100] \times 6.02 \times 10^5}{\text{BET surface area (m}^2/\text{g}) \times 231.84} \quad (1)$$

3.2. Structural properties of the catalysts

XRD patterns of the calcined catalysts are displayed in Fig. 2. All the catalysts showed the diffraction peaks of γ -Al₂O₃ ($2\theta = 37.4$, 46.0 and 67.0°). With the increase of W density, these peak intensities for γ -Al₂O₃ decreased notably. This phenomenon was due to the coverage of WO_x on the alumina surface. Two diffraction peaks at 35.6° and 38.8° ascribed to CuO were detected. The peak intensities declined with increasing W density and even disappeared on Cu-WO_x(0.8)/Al₂O₃. The results indicated that the doping of WO_x promoted the dispersion of Cu. However, the results were opposite

Table 1

The physicochemical properties of the calcined Cu-WO_x/Al₂O₃ catalysts.

Catalyst	Metal loading (mmol/gCat) ^a		ρ_w (W/nm ²)	S_{BET} (m ² /g) ^b	V_p (cm ³ /g) ^b	D_p (nm) ^b	S_{Cu} (m ² /gCat.) ^c	NH ₃ (μ mol/g) ^d
	Cu	W						
Cu/Al ₂ O ₃	0.79	–	–	175.6	0.45	7.5	9.6	49.4
Cu-WO _x (0.2)/Al ₂ O ₃	0.77	0.05	0.2	178.9	0.44	7.2	7.1	50.6
Cu-WO _x (0.4)/Al ₂ O ₃	0.78	0.13	0.4	189.6	0.43	6.6	6.9	56.6
Cu-WO _x (0.6)/Al ₂ O ₃	0.76	0.21	0.6	211.6	0.41	5.9	6.1	68.2
Cu-WO _x (0.8)/Al ₂ O ₃	0.77	0.30	0.8	218.7	0.40	5.7	6.0	73.6

^a Metal loading determined using ICP.

^b BET method.

^c Calculated from the N₂O-TPD results.

^d Calculated by NH₃-TPD.

Table 2

Peak-fitting results of W 4f XPS spectra of catalysts.

Sample	Binding energy for W 4f (eV)				$W^{5+}/(W^{5+} + W^{6+})^a$
	W^{6+} (W 4f _{5/2})	W^{6+} (W 4f _{7/2})	W^{5+} (W 4f _{5/2})	W^{5+} (W 4f _{7/2})	
Cu-WO _x (0.2)/Al ₂ O ₃	40.0	37.9	37.1	35.0	0.42
Cu-WO _x (0.4)/Al ₂ O ₃	39.5	37.4	37.2	35.1	0.44
Cu-WO _x (0.6)/Al ₂ O ₃	39.2	37.1	37.0	34.9	0.47
Cu-WO _x (0.8)/Al ₂ O ₃	39.1	37.0	37.0	34.9	0.48
WO _x (0.6)/Al ₂ O ₃	40.0	37.9	37.8	35.7	0.50
G-WO _x (0.6)/Al ₂ O ₃	40.1	38.0	37.8	35.7	0.57

^a Calculated according to the curve-fitting results of the W 4f XPS spectra of catalysts.

to the N₂O chemisorption results, which showed that the Cu surface area decreased with increasing W density. This observation suggests perimeter of the copper particle was partially decorated with WO_x species, which have both dispersed effect and coverage effect on Cu [31]. The XRD patterns did not show any information about WO_x species, which indicates the high dispersion of WO_x on the catalyst surface.

Raman spectroscopy is suitable for the discrimination of tungsten oxide species such as isolated surface WO₄ species, polytungstate species, WO₃ crystalline NPs, which is strongly dependent on the surface W density [31–33]. The Raman spectra of Cu-WO_x/Al₂O₃ catalysts are shown in Fig. 3. The γ-Al₂O₃ support has no Raman active modes [34]. Cu/Al₂O₃ catalyst presented three characteristic bands of CuO at 293, 341, 629 cm⁻¹. As the W density increasing, the intensity of these bands decreased obviously and almost disappeared when W density increasing to 0.6 W/nm². It confirms that the addition of WO_x promoted the dispersion of

CuO particles. The Cu-WO_x/Al₂O₃ catalysts presented a band at 945 cm⁻¹. This band was ascribed to the symmetric W=O stretching vibration mode of distorted isolated WO₄ tetrahedra [34–36]. Furthermore, no shift of the surface W=O band was observed with increasing W density, which indicates that no polymerized WO_x species existed in all the Cu-WO_x/Al₂O₃ catalysts [24]. The absence of Raman bands in the 500–700 cm⁻¹ region reflected the absence or negligible proportion of bridge W—O—W bond in the catalysts [37], which confirms the isolated WO₄ structure of WO_x species on the catalyst surface.

UV-vis DRS is another useful tool to differentiate tungsten oxide species deposited on Al₂O₃ surface. As shown in Fig. 4, only a single ligand-to-metal charge transfer (LMCT) band at 232 nm was observed in the UV-vis DRS spectra of the Cu-WO_x/Al₂O₃ catalysts, which is the unique feature of UV-vis DRS for the isolated WO₄ reference compounds [37]. It confirms the result that only isolated WO₄ species are present on the Cu-WO_x/Al₂O₃ catalyst.

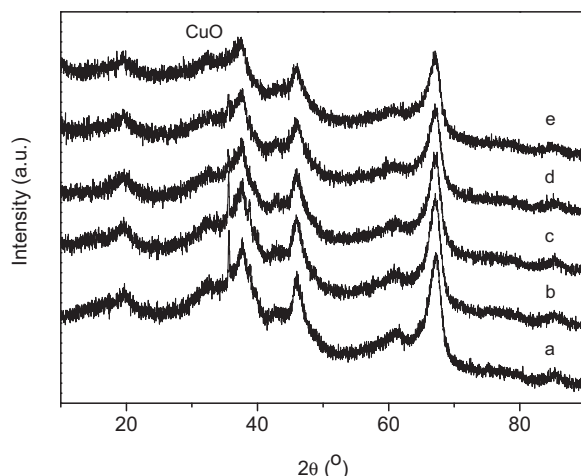


Fig. 2. XRD patterns of calcined Cu-WO_x/Al₂O₃ catalysts: (a) Cu/Al₂O₃, (b) Cu-WO_x(0.2)/Al₂O₃, (c) Cu-WO_x(0.4)/Al₂O₃, (d) Cu-WO_x(0.6)/Al₂O₃, (e) Cu-WO_x(0.8)/Al₂O₃.

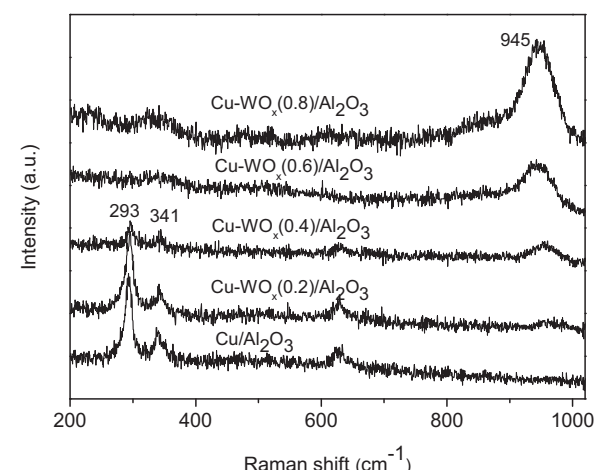


Fig. 3. Raman spectra of the calcined Cu-WO_x/Al₂O₃ catalysts.

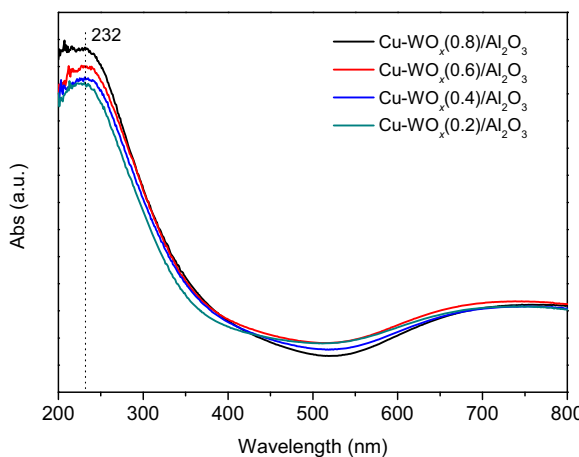


Fig. 4. UV-vis DRS spectra of the calcined Cu-WO_x/Al₂O₃ catalysts.

3.3. Chemical state of the Cu-WO_x/Al₂O₃ catalysts

XPS analysis of binding energies and intensities of the surface species provides information on chemical state and relative quantities of the surface species. Fig. 5A shows the W 4f XPS spectra of the different calcined Cu-WO_x/Al₂O₃ catalysts. All the catalysts show two broad XPS peaks in the range of 32–42 eV. Deconvolutions were performed to distinguish WO_x species in different chemical states from the position of the W 4f level by a curve-fitting procedure. The deconvoluted results shows two doublets with the W 4f_{7/2} B.E. values at 35.0 and 37.1 eV, which are ascribed to W⁵⁺ and W⁶⁺ species [38,39]. Table 2 also gives the quantitative results of the molar ratio of W⁵⁺/(W⁵⁺+W⁶⁺). The results displays that the surface W⁵⁺ species contents increased with increasing WO_x density, which indicates that electronic interactions exist between Cu and WO_x with an intimate contact [30]. The photoelectron peak at 932.9 eV with a strong satellite peak at ca. 943 eV in Cu 2p_{3/2} region (Fig. 5B) suggests that the predominant species is CuO on the calcined Cu-WO_x/Al₂O₃ surface [40]. Furthermore, the Cu 2p_{3/2} XPS spectra and Cu LMM XAES spectra of the reduced Cu/Al₂O₃ and Cu-WO_x(0.8)/Al₂O₃ catalysts were also recorded to confirm the electronic interaction between Cu and WO_x species (Fig. 5C and D). The photoelectron peak at 932.3 eV without the presence of satellite peak indicates that Cu²⁺ was reduced to Cu⁰ and/or Cu⁺, which could be further differentiated through XAES spectra [41]. The Cu LMM XAES spectra show that the relative amount of Cu⁺ to (Cu⁺+Cu⁰) increased with the addition of WO_x species. The results confirm that strong electronic interaction is present between Cu and WO_x species.

3.4. Reducibility and surface acidic properties

In order to reveal the reduction performance of these catalysts, the H₂-TPR profiles were measured. As displayed in Fig. 6, the Cu/Al₂O₃ catalyst showed a strong reduction peak at around 226 °C and a weak shoulder peak at 276 °C. The peak at lower temperature was assigned to the reduction of higher dispersed CuO, while the peak at higher temperature was ascribed to the reduction of large CuO particles with slightly interaction with the support, as reported previously [11,42]. Furthermore, the reduction of the bulk CuO particles was also performed, which displayed an even higher reduction temperature at about 344 °C. With the increase of W density, the intensity of the peak at higher temperature decreased gradually, indicating the decrease of the amount of large CuO particles. The result was consistent with the XRD and Raman results. The low temperature peak at about 226 °C shifted to a higher

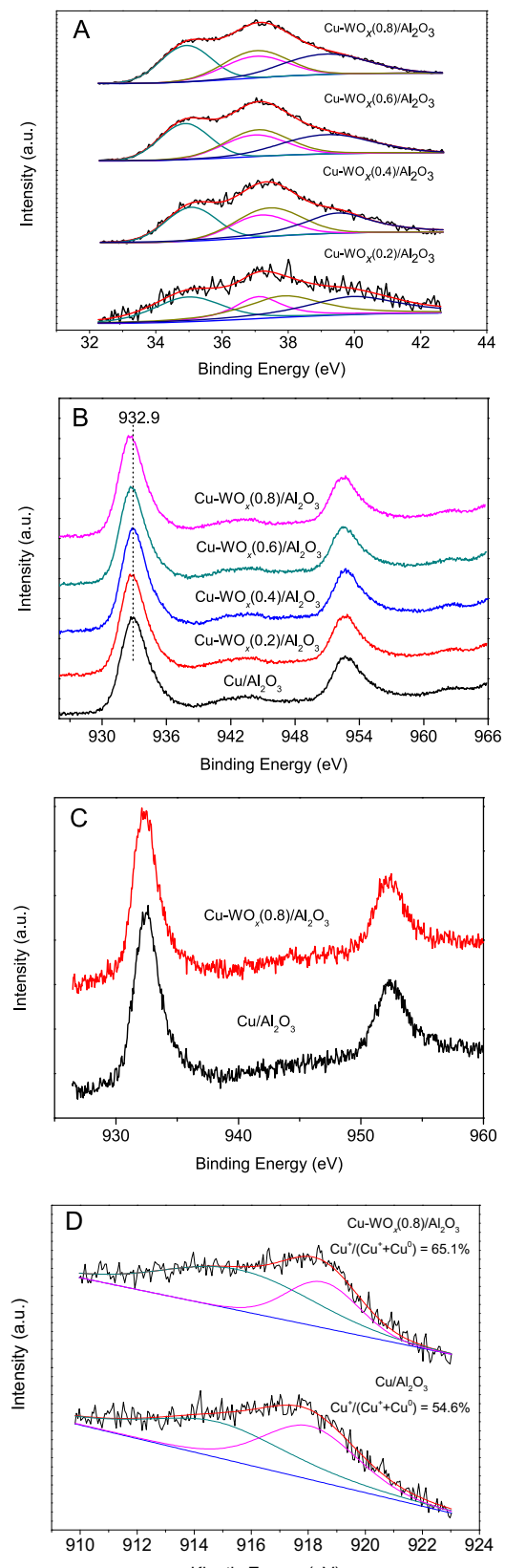


Fig. 5. (A) W 4f XPS spectra and (B) Cu 2p XPS spectra of the calcined Cu-WO_x/Al₂O₃ catalysts, (C) Cu 2p XPS spectra and (D) Cu LMM XAES spectra of the reduced Cu/Al₂O₃ and Cu-WO_x(0.8)/Al₂O₃ catalysts.

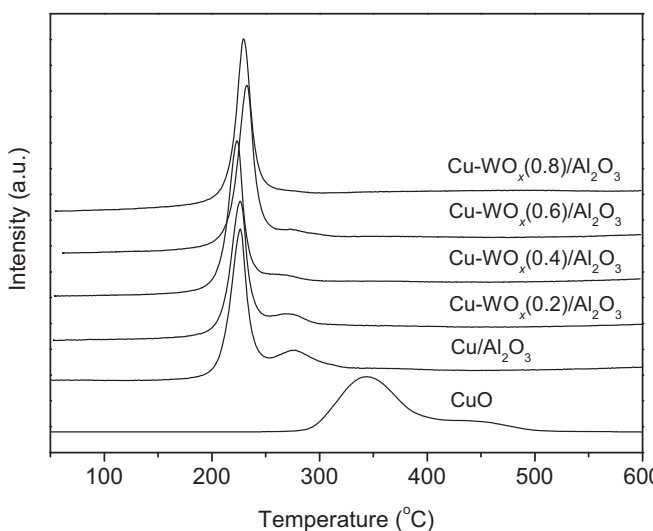


Fig. 6. H_2 -TPR profiles of the $\text{Cu}-\text{WO}_x/\text{Al}_2\text{O}_3$ catalysts.

temperature when W density increased to 0.6 and 0.8 W/nm^2 . It was reported that the highly interacting Cu^{2+} species were more difficult to be reduced than the weakly interacted CuO particles [42]. Therefore, the shift of the reduction temperature could be due to the strong electronic interactions between CuO and WO_x . These results were correlated well with the XRD and XPS results. No reduction peak of WO_x was detected below 600 °C. Horsley reported that the highly dispersed WO_x species were not easily reduced, and the reduction temperature was often above 900 °C according to the literature [33,39].

It is well known that the catalyst acidity plays an important role in determining the product distribution in polyols hydrogenolysis [18,19]. Thus, NH_3 -TPD performances were conducted, as shown in Fig. 7A. The desorbed NH_3 was monitored with a MS detector. In order to eliminate the effect of water (Fig. S1), iron current at m/z 16 was used to calculate the desorbed NH_3 amount. $\text{Cu}/\text{Al}_2\text{O}_3$ showed a broad peak from 130 to 400 °C which centered at 190 °C, revealing that the surface acid strength has a wide distribution on the catalyst [43]. The main ammonia desorption peak before 350 °C was attributed to weak acid sites while the small ammonia desorption peak in the range of 350–400 °C was attributed to stronger acid sites [44]. The results showed that there were mainly weak acid sites on the $\text{Cu}-\text{WO}_x/\text{Al}_2\text{O}_3$ catalysts. The ammonia desorption intensity improved gradually with increasing surface W density. The concentration of the total acid amount per gram of catalyst gives the following increasing order: $\text{Cu}/\text{Al}_2\text{O}_3 < \text{Cu}-\text{WO}_x(0.2)/\text{Al}_2\text{O}_3 < \text{Cu}-\text{WO}_x(0.4)/\text{Al}_2\text{O}_3 < \text{Cu}-\text{WO}_x(0.6)/\text{Al}_2\text{O}_3 < \text{Cu}-\text{WO}_x(0.8)/\text{Al}_2\text{O}_3$.

The Py-FTIR spectra of reduced catalysts evacuated at 30 °C and 350 °C were recorded to measure the acidity of $\text{Cu}-\text{WO}_x/\text{Al}_2\text{O}_3$ catalysts, as shown in Fig. 7B. The bands at 1447 cm^{-1} , 1489 cm^{-1} and 1610 cm^{-1} were indicative of coordination of Py molecules to Lewis acid sites and consequent formation of LPy species. Moreover, the decrease of the intensity and the increase in the frequency of the maximum after evacuation at subsequent higher temperatures indicate that there are both weak and strong Lewis acid sites on the surface of the samples [45,46]. No band at 1540 cm^{-1} was detected in the spectra of the $\text{Cu}-\text{WO}_x/\text{Al}_2\text{O}_3$ catalysts, indicating the absence of Brønsted acid sites on the catalyst surface. The generated Lewis acid sites can be ascribed to the coordinatively unsaturated W^{x+} cations [34]. It is reported that the surface W density plays a key role in the formation of Brønsted acid sites which requires the delocalization of the negative charge. However, the isolated WO_x species cannot delocalize the negative charge, while it occurs over the extended network of polyanstate species [30]. Herein, it can

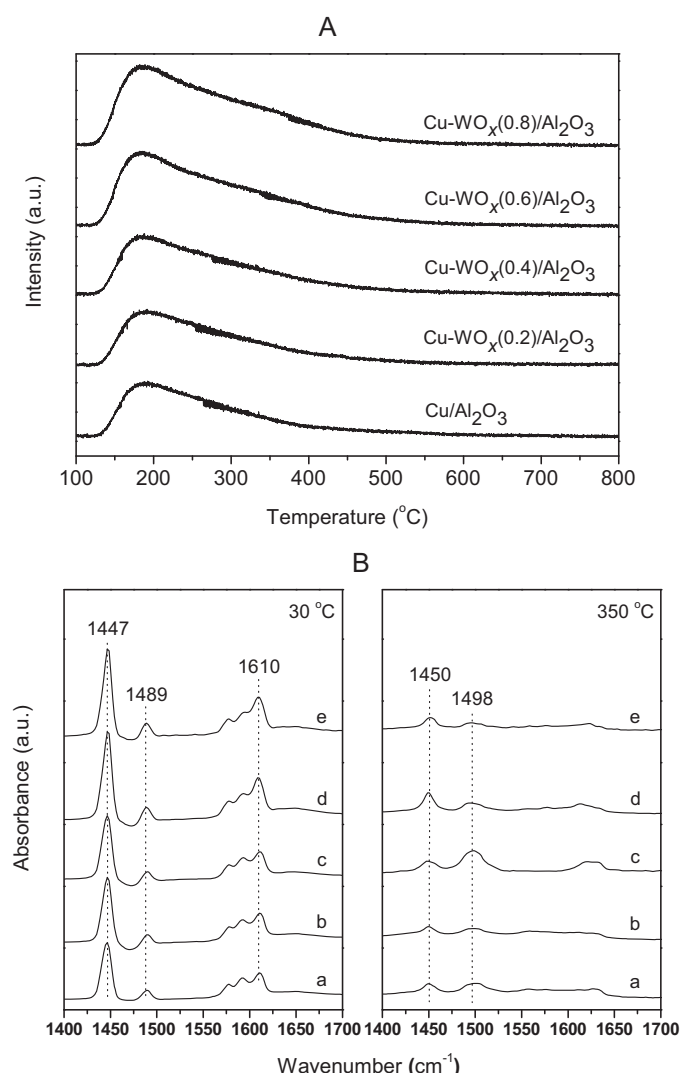


Fig. 7. (A) NH_3 -TPD and (B) Py-FTIR patterns of the reduced $\text{Cu}-\text{WO}_x/\text{Al}_2\text{O}_3$ catalysts: (a) $\text{Cu}/\text{Al}_2\text{O}_3$, (b) $\text{Cu}-\text{WO}_x(0.2)/\text{Al}_2\text{O}_3$, (c) $\text{Cu}-\text{WO}_x(0.4)/\text{Al}_2\text{O}_3$, (d) $\text{Cu}-\text{WO}_x(0.6)/\text{Al}_2\text{O}_3$, (e) $\text{Cu}-\text{WO}_x(0.8)/\text{Al}_2\text{O}_3$.

be the explanation for the absence of Brønsted acid sites at low W surface density.

3.5. The hydrogenolysis of glucose on $\text{Cu}-\text{WO}_x/\text{Al}_2\text{O}_3$ catalysts

The hydrogenolysis of glucose was performed in a continuous fixed-bed reactor at 180 °C and 4 MPa, as shown in Fig. 8 and Table 3. In the conversion of glucose, only polyols were detected in the liquid products. Moreover, sorbitol, glycerol and 1,2-PDO were the main products, small amount of other polyols such as erythritol, EG, 1,2-butanediol (1,2-BDO) and ethanol were observed, while trace amount of isopropanol, propanol and 2-butanol were also detected. It was interesting to note that all the polyols were C_2 , C_3 , C_4 and C_6 products, no product with one or five carbon numbers was detected. Moreover, no product was detected in gas phase. It is inferred that the C–C bond cleavage occurs mainly at C_2-C_4 or C_3-C_3 bond.

The doping of WO_x on the $\text{Cu}-\text{WO}_x/\text{Al}_2\text{O}_3$ catalysts influenced not only the activity of glucose hydrogenolysis but also the selectivity of products. The conversion of glucose as a function of WHSV is illustrated in Fig. 8A. The activity of glucose conversion increased first and then decreased slightly with increasing W density. Both the selectivities of sorbitol and glycerol showed

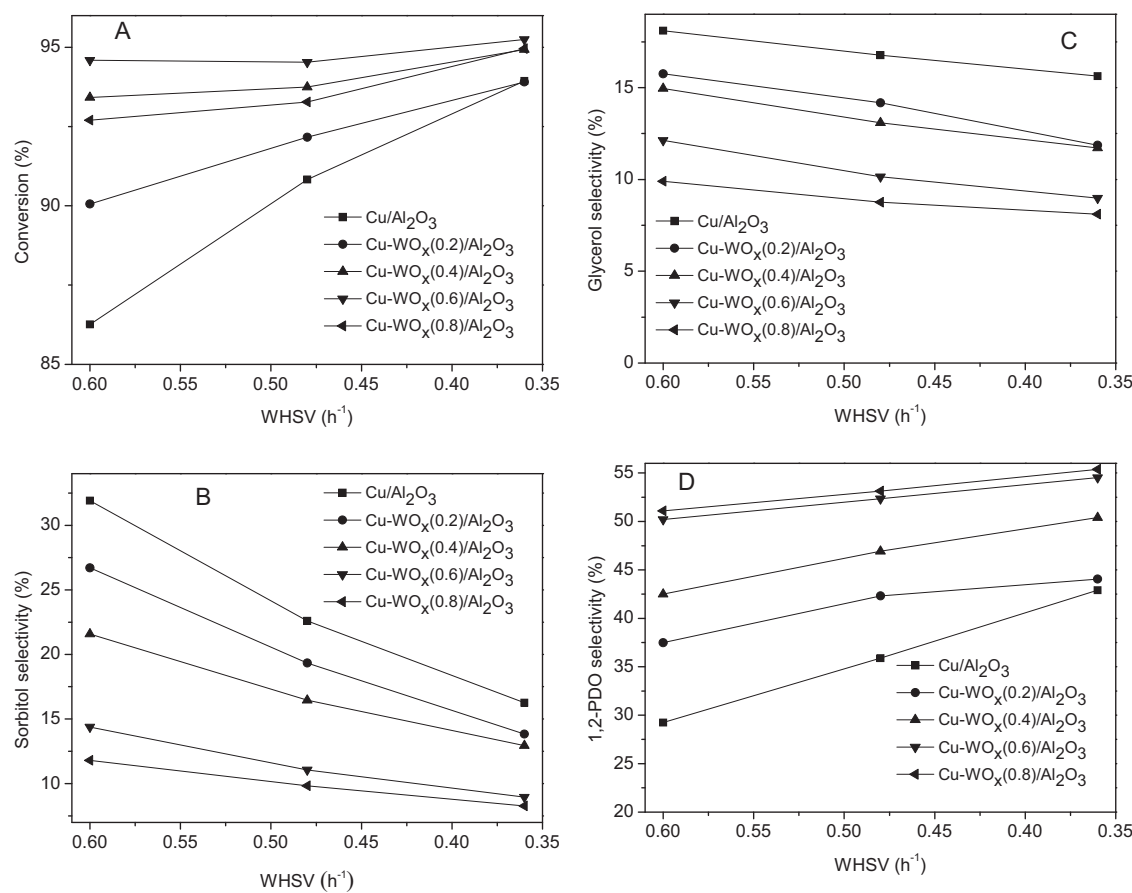


Fig. 8. (A) Glucose conversion, (B) sorbitol selectivity, (C) glycerol selectivity and (D) 1,2-PDO selectivity in glucose hydrogenolysis on the Cu-WO_x/Al₂O₃ catalysts.

an obvious decrease with the increase of W density (Fig. 8B and C). However, as shown in Fig. 8D, the selectivity of 1,2-PDO showed a completely opposite changing trend, which increased with increasing W density. The highest 1,2-PDO selectivity of 55.4% was obtained at WHSV = 0.36 h⁻¹ on Cu-WO_x(0.8)/Al₂O₃ with glucose conversion of 95.0%, which is one of the best performances reported in this reaction. This information suggested that the doping of WO_x promoted the conversion of glucose and the selectivity of 1,2-PDO.

3.6. Correlation between the properties and performance of the Cu-WO_x/Al₂O₃ catalysts

Tomishige's work has shown that transition metals such as Pt, Rh, and Ir have strong interactions with MO_x (W, Mo, Re and so on), and the combination of metal sites and metal oxide species is efficient to the hydrogenolysis of C–O bond [47–53]. In this work, the N₂O-TPD, XRD, Raman, H₂-TPR, and XPS results turn out that WO_x species have coverage, dispersion, and electronic effects on

Table 3

The product distribution of glucose hydrogenolysis on Cu-WO_x/Al₂O₃ catalysts.^a

Catalyst	WHSV (h ⁻¹)	Conv. (%)	Selectivity (%)							
			Sorbitol	Erythritol	EG	Glycerol	1,2-PDO	1,2-BDO	Ethanol	Others ^b
Cu/Al ₂ O ₃	0.60	86.3	31.9	5.1	6.6	18.1	29.2	2.7	1.7	4.7
	0.48	90.8	22.6	4.7	7.2	16.8	35.9	3.8	2.1	6.9
	0.36	93.9	16.3	4.3	8.1	15.9	43.0	4.6	2.4	5.4
Cu-WO _x (0.2)/Al ₂ O ₃	0.60	90.1	26.7	5.3	7.2	15.8	37.5	3.1	2.1	2.3
	0.48	92.2	19.3	4.9	7.5	14.2	42.3	4.3	2.1	5.4
	0.36	93.9	13.8	4.2	7.4	11.9	44.0	5.0	2.3	11.4
Cu-WO _x (0.4)/Al ₂ O ₃	0.60	93.4	21.6	5.5	8.1	15.0	42.5	4.4	1.9	1.0
	0.48	93.7	16.5	5.1	8.1	13.1	46.9	5.4	2.6	2.3
	0.36	94.9	12.9	4.7	8.2	11.7	50.4	6.2	3.5	2.4
Cu-WO _x (0.6)/Al ₂ O ₃	0.60	94.6	14.4	5.5	8.5	12.1	50.2	6.0	2.2	1.1
	0.48	94.5	11.1	5.0	8.1	10.1	52.3	7.0	4.0	2.4
	0.36	95.2	9.0	4.3	8.0	9.0	54.5	8.0	3.7	3.5
Cu-WO _x (0.8)/Al ₂ O ₃	0.60	92.7	11.8	5.5	8.0	9.9	51.1	7.0	2.6	4.1
	0.48	93.3	9.8	5.0	7.8	8.8	52.1	7.5	4.6	4.4
	0.36	95.0	8.3	4.4	8.0	8.1	55.4	8.5	3.8	3.5

^a Reaction conditions: 4 MPa H₂, 180 °C, 5 wt% glucose aqueous solution.

^b Others: isopropyl alcohol, propanol, 2-butanol, humins, etc.

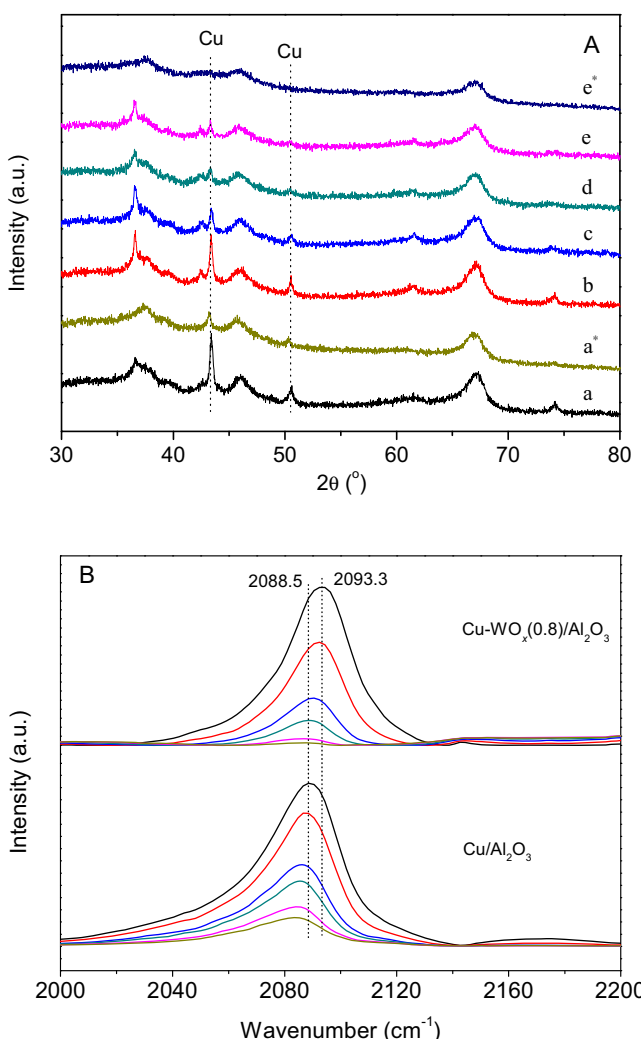


Fig. 9. (A) The XRD patterns of the spent (a, b, c, d, e) and reduced (a*, e*) $\text{Cu}-\text{WO}_x/\text{Al}_2\text{O}_3$ catalysts and (B) CO-FTIR of the reduced $\text{Cu}/\text{Al}_2\text{O}_3$ and $\text{Cu}-\text{WO}_x(0.8)/\text{Al}_2\text{O}_3$ catalysts. (a) $\text{Cu}/\text{Al}_2\text{O}_3$, (b) $\text{Cu}-\text{WO}_x(0.2)/\text{Al}_2\text{O}_3$, (c) $\text{Cu}-\text{WO}_x(0.4)/\text{Al}_2\text{O}_3$, (d) $\text{Cu}-\text{WO}_x(0.6)/\text{Al}_2\text{O}_3$, (e) $\text{Cu}-\text{WO}_x(0.8)/\text{Al}_2\text{O}_3$, (a*) $\text{Cu}/\text{Al}_2\text{O}_3$, (e*) $\text{Cu}-\text{WO}_x(0.8)/\text{Al}_2\text{O}_3$. a* and e* were reduced at 250°C for 2 h with a ramp rate of $1^\circ\text{C}/\text{min}$, and protected with liquid paraffin.

copper sites. The XRD patterns of the reduced and used catalysts were also obtained to confirm the strong interaction between Cu sites and WO_x species (Fig. 9A). The results show that the diffraction peaks at 43.3 and 50.5° are present on the used catalysts which can be ascribed to Cu^0 . Furthermore, the intensity of the two peaks decreased with the increasing WO_x surface density. The XRD pattern of the reduced $\text{Cu}/\text{Al}_2\text{O}_3$ catalyst also shows the Cu^0 diffraction peaks. However, the diffraction peaks of Cu^0 disappeared in the XRD pattern of $\text{Cu}-\text{WO}_x(0.8)/\text{Al}_2\text{O}_3$ catalyst. These XRD results confirm that WO_x species have dispersion effect on Cu particles. The CO-FTIR spectra of $\text{Cu}/\text{Al}_2\text{O}_3$ and $\text{Cu}-\text{WO}_x(0.8)/\text{Al}_2\text{O}_3$ catalysts were also recorded (Fig. 9B). CO is used as a probe molecular to study the electronic environment of the supported metal. Prior to the measurements, the catalysts were reduced at 250°C for 2 h. Generally, the band in the range of 2025 – 2125 cm^{-1} arises from linear bound CO molecules on different Cu sites with a prevailing metal character [54]. The frequency of CO adsorbed on Cu sites over $\text{Cu}-\text{WO}_x(0.8)/\text{Al}_2\text{O}_3$ catalyst surface shows an obvious blue shift compared with that over $\text{Cu}/\text{Al}_2\text{O}_3$. This may be due to the decrease of electron density in Cu^0 nucleus which is consistent with the XPS results. It suggests that WO_x species have an intimate contact with

Cu metal sites and have an electronic effect on it. The variation of the properties of the $\text{Cu}-\text{WO}_x/\text{Al}_2\text{O}_3$ catalysts could lead to different catalytic performances. As reported by Huber [18,19], the reaction of polyols hydrogenolysis was regulated by the synergistic catalysis of metal and acid sites. A large amount of literature had reported the linear correlation between the ratio of metal surface area/acid amount and its behaviour on polyols hydrogenolysis such as glycerol, dimethyl oxalate hydrogenation, 5-methylfurfuryl alcohol hydrogenolysis, and carbon dioxide hydrogenation to methanol [11,55–57]. For example, a linear relationship between the yield of 1,2-PDO from glycerol and copper metal surface area or the Lewis acid amount was widely reported [11,58]. Moreover, surface copper and Lewis acid sites are important factors in the structure–performance relationship for polyols hydrogenolysis considering their activity on the elemental reactions involving C–C/C–O bond cleavage. The highest 1,2-PDO selectivity on $\text{Cu}-\text{WO}_x(0.8)/\text{Al}_2\text{O}_3$ was suggested to be related with the proper Lewis acid/metal surface molar ratio. A similar relationship between the product selectivity and the ratio of Lewis acid to copper site amount was proposed and shown in Fig. 10A. When $\text{WHSV}=0.6\text{ h}^{-1}$, sorbitol and glycerol selectivities decreased linearly with increasing the molar ratio of Lewis acid to metal sites. Meanwhile, the 1,2-PDO selectivity increased linearly with the increase of the molar ratio of Lewis acid to metal sites. Actually, the correlation between the product selectivities and the molar ratio of Lewis acid to metal sites in $\text{WHSV}=0.48$ and 0.36 h^{-1} also displayed the same linear relationship, as shown in Fig. 10B and Fig. 10C. The correlations strongly suggest that metal and Lewis acid sites are the active sites for glucose hydrogenolysis in H_2 atmosphere, and the proper molar ratio of Lewis acid to metal sites was crucial for the efficient hydrogenolysis of glucose to 1,2-PDO. The correlations also indicate that the increase of molar ratio of Lewis acid to metal sites promotes the cleavage of C–C/C–O bonds. In order to identify the stability and the real acidity of the catalysts in the hydrothermal environment, a special Py-FTIR experiment was designed (Fig. S2 and Table S1 of Supporting Information). The samples were reduced at 250°C in H_2 for 2 h and then degassed to a pressure of 10^{-2} MPa at 350°C for 1 h. After cooling down to 30°C , vapor was adsorbed for 30 min. After evacuation for 30 min, Pyridine was adsorbed for 30 min. The Py-IR spectra were measured at 30°C and 180°C after evacuation for 30 min. The results turn out that very small amount of Brønsted acid sites were generated when the catalysts were exposed to the vapor environment. The ratios of Brønsted to Lewis acid were only 0.091 and 0.018 on $\text{Cu}/\text{Al}_2\text{O}_3$ and $\text{Cu}-\text{WO}_x(0.8)/\text{Al}_2\text{O}_3$, respectively after evacuation at 30°C . The Brønsted acid sites on the surface of the two catalysts nearly disappeared after evacuation at 180°C . The results confirm that Lewis acid sites on $\text{Cu}-\text{WO}_x/\text{Al}_2\text{O}_3$ are the catalytic active sites in the hydrothermal condition. The promoting mechanism of WO_x species on glucose hydrogenolysis to 1,2-PDO will be attempted to discuss below.

3.7. Promoting mechanism of WO_x on glucose hydrogenolysis to 1,2-PDO

The decrease of the selectivities of sorbitol and glycerol and the simultaneous increase of 1,2-PDO selectivity with increasing WHSV indicate that the hydrogenolysis of glucose to 1,2-PDO may be a cascade reaction with sorbitol and glycerol as the intermediates. In order to clear the reaction route of glucose conversion to 1,2-PDO on $\text{Cu}-\text{WO}_x/\text{Al}_2\text{O}_3$, the hydrogenolysis of the intermediates was performed on $\text{Cu}-\text{WO}_x(0.6)/\text{Al}_2\text{O}_3$ at $\text{WHSV}=0.6\text{ h}^{-1}$ (Fig. S3 in Supporting Information). However, $\text{Cu}-\text{WO}_x(0.6)/\text{Al}_2\text{O}_3$ shows no activity for the hydrogenolysis of the saturated polyols such as sorbitol, erythritol, glycerol, 1,2-PDO, and EG. It indicates that the saturated polyols are the terminal products and cannot undergo the hydrogenolysis reaction. So 1,2-PDO did not come from

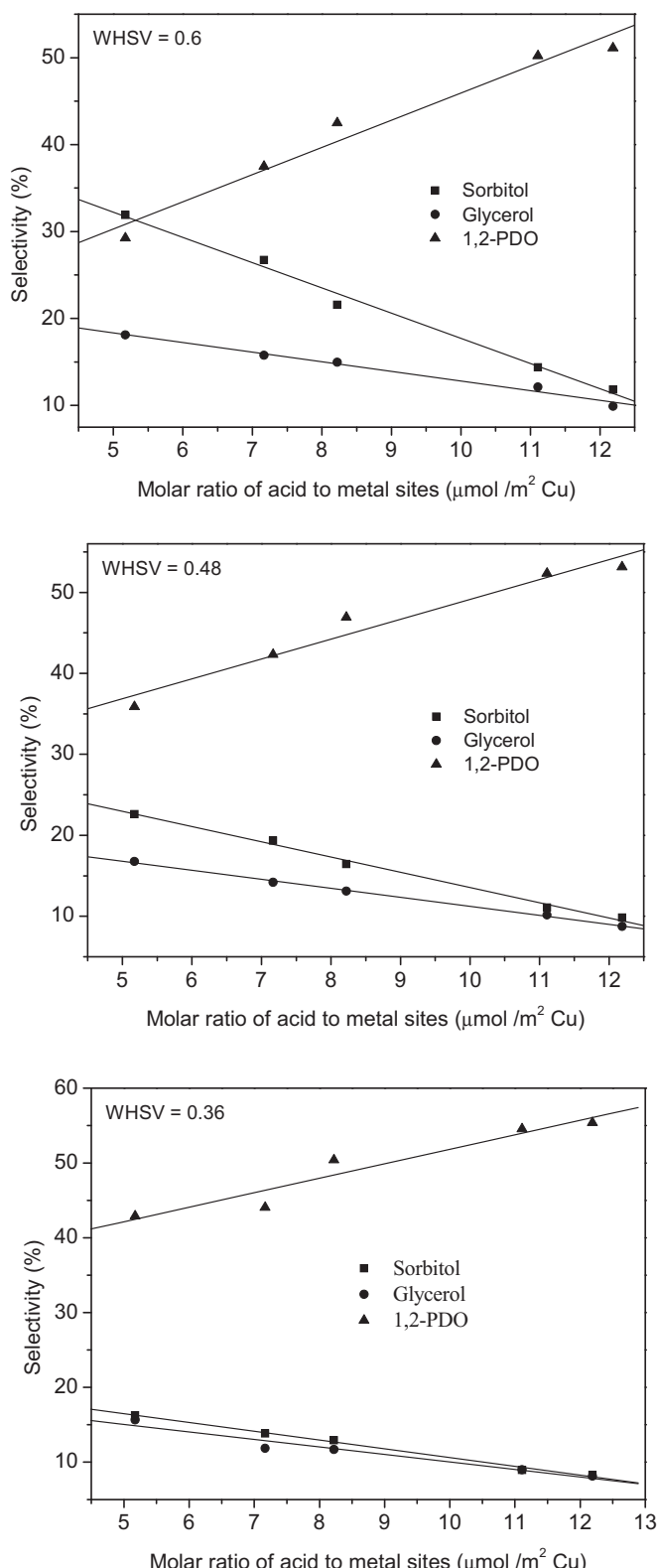


Fig. 10. 1,2-PDO selectivity as a function of the molar ratio of Lewis acid to copper surface area: Reaction condition: 180 °C, 4 MPa, 5 wt% glucose solution, WHSV = 0.6, 0.48, and 0.36 h⁻¹.

the hydrogenolysis of saturated polyols such as sorbitol, erythritol, and glycerol on Cu-WO_x/Al₂O₃. Therefore, sorbitol and glycerol could not be the intermediates for the hydrogenolysis of glucose to 1,2-PDO. In order to examine the activities of Cu/Al₂O₃ and Cu-WO_x/Al₂O₃ for C=O bond hydrogenation, the hydrogenation of

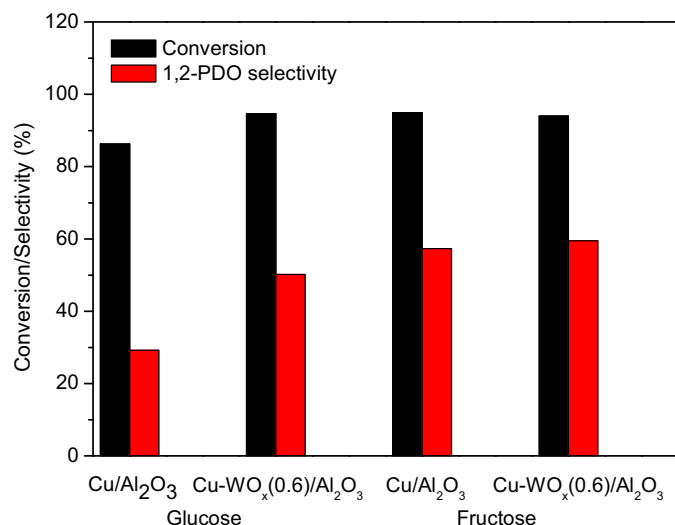
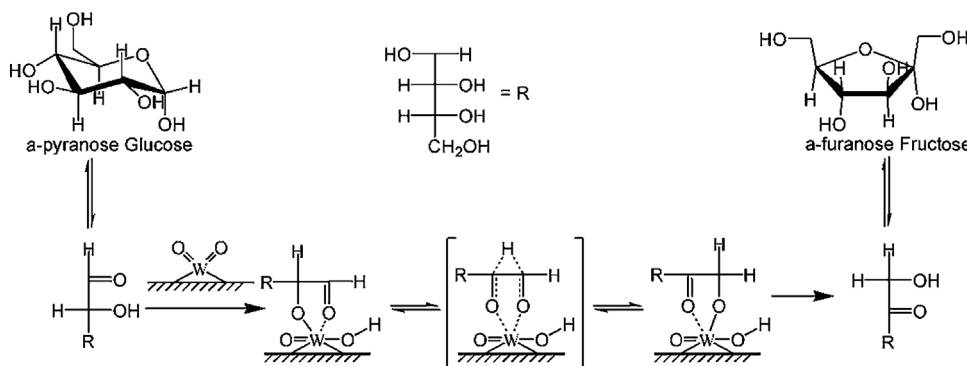


Fig. 11. The hydrogenolysis of glucose and fructose on Cu/Al₂O₃ and Cu-WO_x(0.6)/Al₂O₃.

glucose at a lower temperature of 100 °C was performed (Table S2 of Supporting Information). The results showed that only fructose and sorbitol were produced. Furthermore, the yields of fructose and sorbitol increased with the addition of WO_x species. It suggests that WO_x species can promote the activity of Cu metal sites for C=O bond hydrogenation. The C=O bond hydrogenation activity is related with the interaction between Cu sites and WO_x species. As shown in Table 1, the Cu surface areas decreased with increasing W surface density, indicating the decrease of hydrogenation sites. Therefore, we suppose that the increased hydrogenation activity of Cu may be dependent on the electron interaction between Cu sites and WO_x species as proved by XPS and CO-FTIR results. The isomerization reaction was also promoted by WO_x species. Therefore, the decrease of sorbitol and glycerol selectivities could be due to the promoting effect of WO_x on glucose isomerization to fructose and fructose conversion which is competitive with glucose conversion to sorbitol and glycerol. As mentioned above, the hydrogenolysis of glucose to 1,2-PDO mainly includes two steps: (1) the isomerization of glucose to fructose; (2) the hydrogenolysis of fructose to 1,2-PDO. In order to confirm the reaction route of glucose hydrogenolysis to 1,2-PDO on Cu-WO_x/Al₂O₃ and reveal the effect of WO_x on the different reaction steps of glucose hydrogenolysis, the hydrogenolysis of fructose was conducted on Cu/Al₂O₃ and Cu-WO_x(0.6)/Al₂O₃ at WHSV = 0.6 h⁻¹ in Fig. 11. Compared with glucose hydrogenolysis, Cu/Al₂O₃ shows extremely high conversion and 1,2-PDO selectivity in fructose hydrogenolysis with the value of 94.0% and 57.3%, respectively, which is much higher than that of glucose conversion. It suggests that fructose has high activity and selectivity for 1,2-PDO and the isomerisation of glucose to fructose could be the rate-controlling step in glucose hydrogenolysis to 1,2-PDO on Cu/Al₂O₃. Furthermore, Cu/Al₂O₃ and Cu-WO_x(0.6)/Al₂O₃ show nearly the same fructose conversion (94.0 and 94.9%) and 1,2-PDO selectivity (57.3 and 59.5%). It indicates that the addition of WO_x mainly promotes the isomerization of glucose to fructose and has little effect on fructose hydrogenolysis.

As generally accepted that the isomerization reaction can be promoted by Lewis acid in the catalyst by polarizing the carbonyl group in the ketone [59–61]. Davis et al. [59] showed that Sn incorporated in the framework of zeolite Beta, as Lewis acid, performed the isomerization reaction following an intramolecular hydride shift mechanism between the carbonyl-containing C-1 and hydroxyl-bearing C-2 of glucose by a way of a 5-member complex. As discussed above, the isolated WO₄, as W⁵⁺ or W⁶⁺



Scheme 1. Promoting mechanism of the isolated WO_4 in hexavalent on glucose isomerization to fructose.

species, provides more Lewis acid sites. Therefore, the mechanism of the isomerization of glucose to fructose on W^{x+} may be the same as that on Sn^{x+} considering their same tetrahedral structure and Lewis acid role in the reaction step. The XPS spectra of $\text{WO}_x/\text{Al}_2\text{O}_3$ with/without glucoses adsorption were obtained to explore the exact promoting mechanism, as shown in Fig. 12. Based on the deconvolution of W 4f region of the XPS spectra in the range of 32–42 eV, both the W^{5+} and W^{6+} species existed on the catalyst surface. However, the content of W^{5+} species on $\text{WO}_x/\text{Al}_2\text{O}_3$ with glucoses adsorption was higher than that without glucoses adsorption as shown in Table 2. It seems that WO_x was ‘reduced’ by glucose. Therefore, we suppose that glucose may adsorb on the W^{6+} species and a Glucose- W^{6+} complex is formed. Moreover, the adsorption of glucose on W^{6+} species could promote the isomerization of glucose to fructose. Therefore, the promoting mechanism of W^{6+} species on glucose isomerization was proposed in Scheme 1.

3.8. The possible reaction route of glucose hydrogenolysis on $\text{Cu}-\text{WO}_x/\text{Al}_2\text{O}_3$

The reaction route of glucose hydrogenolysis has been rarely studied. Kanie [62] had studied the hydrogenolysis of glucose on Pt nanoparticles and proposed a reaction route. Based on the model reactions of fructose and glycerol, they suggested that 1,2-PDO was obtained from the hydrogenolysis of glycerol and the unsaturated intermediates that were from the retro-aldol condensation of fructose. In this work, the main reaction pathway of glucose

hydrogenolysis on $\text{Cu}-\text{WO}_x/\text{Al}_2\text{O}_3$ was proposed in Scheme 2 based on the hydrogenolysis of glucose and the intermediates. Partial reaction procedures were similar with those illustrated in supercritical water or subcritical water under hydrogen atmosphere [20,21,62]. The hydrogenation of glucose to sorbitol is a competitive reaction with the isomerization of glucose to fructose and the hydrogenolysis of glucose to lower polyols. It is catalyzed by the hydrogenation of copper. As identified in many reports, the isomerization between glucose and fructose could occur at supercritical/subcritical water even with no catalysts [20]. Furthermore, the isomerization can occur by intramolecular hydride shift in the present of Lewis acid [59,60]. The new Lewis acid produced by WO_x can promote the isomerization of glucose to fructose. As reported previously, the hydrogenation of fructose mainly produced mannitol. However, it could not be differentiated with the sorbitol in our experiments. The retro-aldol reaction of glucose to erythrose and glycolaldehyde and the retro-aldol reaction of fructose to dihydroxyacetone and glyceraldehydes intermediates were performed on the surface copper sites in H_2 atmosphere. The hydrogenation of these unsaturated intermediates to lower polyols such as erythritol, EG, glycerol was also carried out on the copper sites. The dehydration followed by hydrogenation of these intermediates was speculated to be conducted on the acid sites and copper sites, respectively. Polyols such as 1,2-PDO, 1,2-BDO, and erythritol were obtained. It was confirmed that 1,2-BDO and EG did not come from erythritol, which could be from the hydrogenolysis of erythrose and glycolaldehyde, respectively. Furthermore, 1,2-PDO was only from the hydrogenolysis of the dihydroxyacetone and glyceraldehyde, which is different from Kanie’s report.

Regarding the synergy of Cu metal sites and WO_x species on 1,2-PDO selectivity, it is thought that the interface between Cu metal surface and WO_x species could play an important role on C–O bond hydrogenolysis. Tomishige’s group studied the hydrogenolysis of ethers and polyols over $\text{Rh}(\text{Ir})-\text{ReO}_x/\text{SiO}_2$ catalysts and proposed mechanisms of the hydrogenolysis of C–O bond over the metal and metal oxide interface [63–65]. Take the hydrogenolysis of glycerol to 1,2-PDO over $\text{Ir}-\text{ReO}_x/\text{SiO}_2$ for example, the interface between Ir metal surface and ReO_x clusters is the catalytically active site. Glycerol is adsorbed on the ReO_x clusters at the terminal oxygen to form alkoxide species. H_2 is adsorbed on Ir metal sites and dissociated into a proton and a hydride. The hydride species attacks the 3-position of the alkoxide to break the C–O bond. Considering the synergy of Cu and WO_x species on glucose hydrogenolysis, a similar reaction mechanism was proposed and shown in Scheme 3. Tomishige’s group also found out that high valent Re and W was efficient to the removal of two C–O bonds [66,67]. In our work, 1,2-BDO selectivity was also promoted by WO_x species. Therefore, a reasonable mechanism on erythrose hydrogenolysis to 1,2-BDO was proposed and shown in Scheme 4.

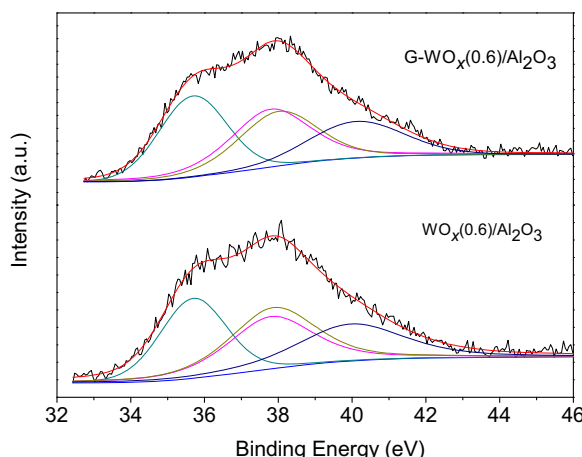
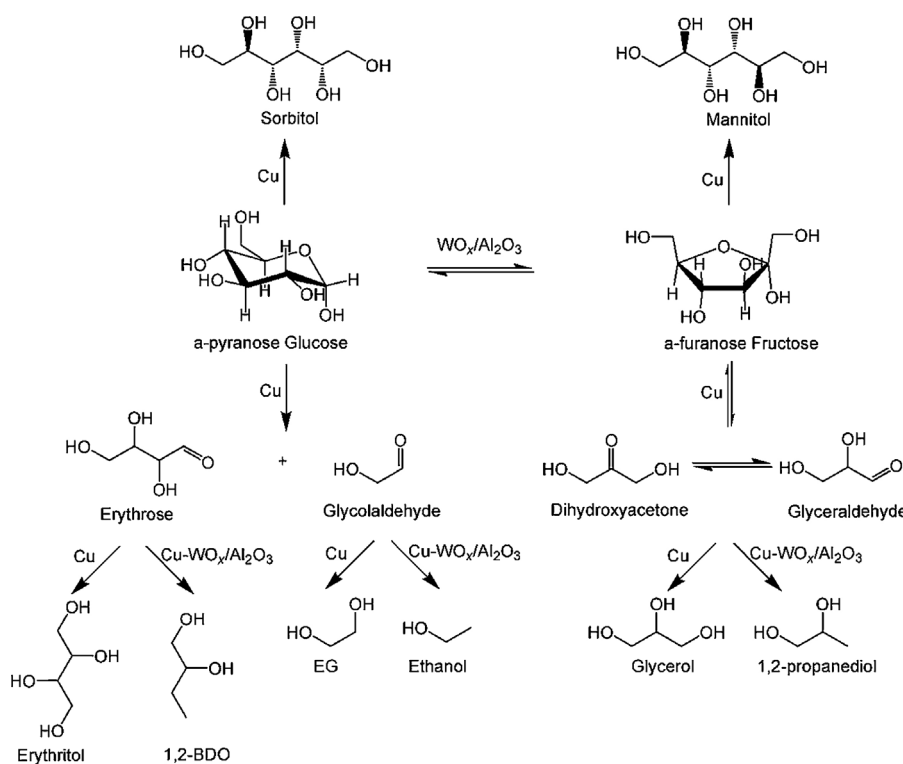
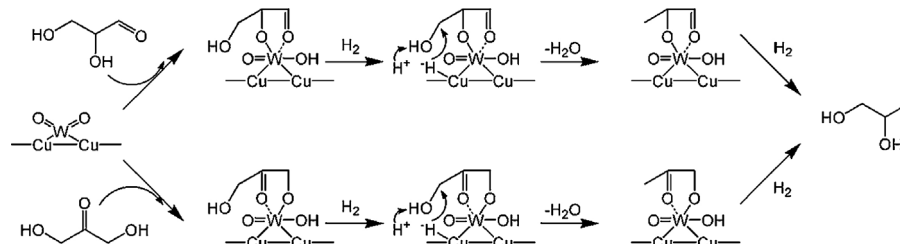


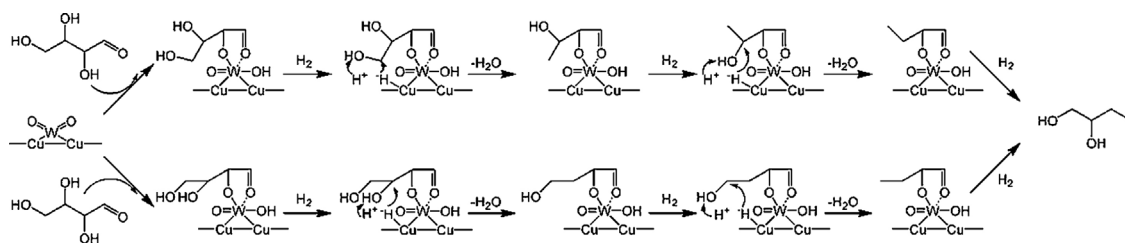
Fig. 12. W 4f XPS spectra of the $\text{WO}_x(0.6)/\text{Al}_2\text{O}_3$ catalyst with/without glucose adsorption.



Scheme 2. The possible reaction route of glucose hydrogenolysis on Cu-WO_x/Al₂O₃.



Scheme 3. Proposed mechanism of dihydroxyacetone and glyceraldehyde hydrogenolysis to 1,2-PDO over Cu-WO_x/Al₂O₃.



Scheme 4. Proposed mechanism of erythrose hydrogenolysis to 1,2-BDO over Cu-WO_x/Al₂O₃.

4. Conclusion

The hydrogenolysis of glucose was conducted on a series of Cu-WO_x/Al₂O₃ catalysts. WO_x species are present on Cu-WO_x/Al₂O₃ as isolated WO₄. The isolated WO₄ species provide more Lewis acid on the catalysts and have shielding, dispersion, electronic effect on Cu sites. A strong correlation between catalyst properties and performance was observed. The selectivity of 1,2-PDO increased linearly with the increase of molar ratio of acid to metal sites, while the selectivity of sorbitol and glycerol decreased

with the increase of the molar ratio of acid to metal sites. The highest 1,2-PDO selectivity was obtained on Cu-WO_x(0.8)/Al₂O₃ at WHSV=0.36 h⁻¹, with the value of 55.4%. The adsorption of glucose on isolated WO₄ in hexavalent promotes the isomerization of glucose to fructose which has higher selectivity to 1,2-PDO. The promoting effect of W⁶⁺ on glucose isomerization to 1,2-PDO was proposed. A proper reaction route of glucose hydrogenolysis on Cu-WO_x/Al₂O₃ in H₂ atmosphere was proposed. The mechanisms of the C–O bond hydrogenolysis were discussed.

Acknowledgement

This work was financially supported by the Major State Basic Research Development Program of China (973 Program) (No. 2012CB215305).

Appendix A. Supplementary data

Supplementary data associated with this article can be found, in the online version, at <http://dx.doi.org/10.1016/j.cattod.2015.06.030>

References

- [1] M.J. Climent, A. Corma, S. Iborra, *Green Chem.* 16 (2014) 516–547.
- [2] A.M. Ruppert, K. Weinberg, R. Palkovits, *Angew. Chem. Int. Ed.* 51 (2012) 2564–2601.
- [3] K. Fabičovcová, O. Malter, M. Lucas, P. Claus, *Green Chem.* 16 (2014) 3580–3588.
- [4] Y. Liao, Q. Liu, T. Wang, J. Long, L. Ma, Q. Zhang, *Green Chem.* 16 (2014) 3305–3312.
- [5] W. Zhu, H. Yang, J. Chen, C. Chen, L. Guo, H. Gan, X. Zhao, Z. Hou, *Green Chem.* 16 (2014) 1534–1542.
- [6] J.N. Chheda, G.W. Huber, J.A. Dumesic, *Angew. Chem. Int. Ed.* 46 (2007) 7164–7183.
- [7] G.W. Huber, S. Iborra, A. Corma, *Chem. Rev.* 106 (2006) 4044–4098.
- [8] A. Corma, S. Iborra, A. Velty, *Chem. Rev.* 107 (2007) 2411–2502.
- [9] M.E. Zakrzewska, E. Bogel-Lukasik, R. Bogel-Lukasik, *Chem. Rev.* 111 (2011) 397–417.
- [10] J. Song, H. Fan, J. Ma, B. Han, *Green Chem.* 15 (2013) 2619–2635.
- [11] S. Zhu, X. Gao, Y. Zhu, H. Zheng, Y. Li, *J. Catal.* 303 (2013) 70–79.
- [12] L. Ye, X. Duan, H. Lin, Y. Yuan, *Catal. Today* 183 (2012) 65–71.
- [13] X. Chen, X. Wang, S. Yao, X. Mu, *Catal. Commun.* 39 (2013) 86–89.
- [14] M. Banu, S. Sivasanker, T.M. Sankaranarayanan, P. Venuvanalingam, *Catal. Commun.* 12 (2011) 673–677.
- [15] W.H. Zartman, H. Adkins, *J. Am. Chem. Soc.* 55 (1933) 4559–4563.
- [16] Z. Xiao, S. Jin, M. Pang, C. Liang, *Green Chem.* 15 (2013) 891–895.
- [17] N. Li, G.W. Huber, *J. Catal.* 270 (2010) 48–59.
- [18] Y.T. Kim, J.A. Dumesic, G.W. Huber, *J. Catal.* 304 (2013) 72–85.
- [19] G.W. Huber, J.W. Shabaker, S.T. Evans, J.A. Dumesic, *Appl. Catal. B: Environ.* 62 (2006) 226–235.
- [20] M. Holm, S. Saravanamurugan, E. Taarning, *Science* 328 (2010) 602–605.
- [21] M. Sasaki, K. Goto, K. Tajima, T. Adscharina, K. Arai, *Green Chem.* 4 (2002) 285–287.
- [22] Z. Huang, J. Chen, Y. Jia, H. Liu, C. Xia, H. Liu, *Appl. Catal. B: Environ.* 147 (2014) 377–386.
- [23] X. Chen, G. Clet, K. Thomas, M. Houalla, *J. Catal.* 273 (2010) 236–244.
- [24] T. Kim, A. Burrows, C.J. Kiely, I.E. Wachs, *J. Catal.* 246 (2007) 370–381.
- [25] B. Zhang, Y. Zhu, G. Ding, H. Zheng, Y. Li, *Appl. Catal. A: Gen.* 443–444 (2012) 191–201.
- [26] C.J.G. Van Der Grift, A.F.H. Wielers, B.P.J. Jogh, J. Van Beunum, M. De Boer, M. Versluijs-Helder, W. Geus, *J. Catal.* 131 (1991) 178–189.
- [27] W.L. Chu, T. Echizen, Y. Kamiy, T. Okuhara, *Appl. Catal. A: Gen.* 259 (2004) 199–205.
- [28] S. Chen, W. Wang, Y. Zhang, Y. Wei, W. Fang, Y. Yang, *J. Mol. Catal. A: Chem.* 365 (2012) 60–65.
- [29] D.G. Barton, S.L. Soled, G.D. Meitzner, G.A. Fuentes, E. Iglesia, *J. Catal.* 181 (1999) 57–72.
- [30] S. García-Fernández, I. Gandarias, J. Requies, M.B. Güemez, S. Bennici, A. Auroux, P.L. Arias, *J. Catal.* 323 (2015) 65–75.
- [31] Y. Hong, D. Lee, H. Eom, K. Lee, *Appl. Catal. B: Environ.* 150–151 (2014) 438–445.
- [32] S.S. Chan, I.E. Wachs, L.L. Murrell, N.C. Dispensiere, *J. Catal.* 92 (1985) 1–10.
- [33] J.A. Horsley, I.E. Wachs, J.M. Brown, G.H. Via, F.D. Hardcastle, *J. Phys. Chem.* 91 (1987) 4014–4020.
- [34] X. Wu, L. Zhang, D. Weng, S. Liu, Z. Si, J. Fan, *J. Hazard. Mater.* 225–226 (2012) 146–154.
- [35] R. Moraesa, K. Thomasa, S. Thomasa, S.V. Donkb, G. Grasso, J.P. Gilsona, M. Houallaa, *J. Catal.* 286 (2012) 62–77.
- [36] N. Liu, S. Ding, Y. Cui, N. Xue, L. Peng, X. Guo, W. Ding, *Chem. Eng. Res. Des.* 91 (2013) 573–580.
- [37] E.I. Ross-Medgaarden, I.E. Wachs, *J. Phys. Chem. C* 111 (2007) 15089–15099.
- [38] M. Occhiuzzi, D. Cordischi, D. Gazzoli, M. Valigi, P.C. Heydorn, *Appl. Catal. A: Gen.* 269 (2004) 169–177.
- [39] X. Yang, R. Gao, W. Dai, K. Fan, *J. Phys. Chem. C* 112 (2008) 3819–3826.
- [40] A.J. McCue, C.J. McRitchie, A.M. Shepherd, J.A. Anderson, *J. Catal.* 319 (2014) 127–135.
- [41] G. Corro, S. Cebada, U. Pal, J.L.G. Fierro, J. Alvarado, *Appl. Catal. B: Environ.* 165 (2015) 555–565.
- [42] Z. Huang, F. Cui, H. Kang, J. Chen, C. Xia, *Appl. Catal. A: Gen.* 366 (2009) 288–298.
- [43] A.H. Karima, S. Triwahyonoa, A.A. Jalilb, H. Hattori, *Appl. Catal. A: Gen.* 433–434 (2012) 49–57.
- [44] L. Vilcocq, R. Koerin, A. Cabiac, C. Espezel, S. Lacombe, D. Duprez, *Appl. Catal. B: Environ.* 148–149 (2014) 499–508.
- [45] M.I. ZaKi, M.A. Hasan, F.A. Al-Sagheer, L. Pasupulety, *Colloid. Surf. A* 190 (2001) 261–274.
- [46] P. Concepción, M.T. Navarro, T. Blasco, J.M. López Nieto, B. Panzacchi, F. Rey, *Catal. Today* 96 (2004) 179–186.
- [47] K. Chen, S. Koso, T. Kubota, Y. Nakagawa, K. Tomishige, *ChemCatChem* 2 (2010) 547–555.
- [48] Y. Amada, S. Koso, Y. Nakagawa, K. Tomishige, *ChemSusChem* 3 (2010) 728–736.
- [49] Y. Amada, Y. Shinmi, S. Koso, T. Kubota, Y. Nakagawa, K. Tomishige, *Appl. Catal. B: Environ.* 105 (2011) 117–127.
- [50] S. Koso, H. Watanabe, K. Okumura, Y. Nakagawa, K. Tomishige, *Appl. Catal. B: Environ.* 111–112 (2012) 27–37.
- [51] Y. Amada, H. Watanabe, M. Tamura, Y. Nakagawa, K. Okumura, K. Tomishige, *J. Phys. Chem. C* 116 (2012) 23503–23514.
- [52] T. Ebashi, Y. Ishida, Y. Nakagawa, S. Ito, T. Kubota, K. Tomishige, *J. Phys. Chem. C* 114 (2010) 6518–6526.
- [53] S. Koso, H. Watanabe, K. Okumura, Y. Nakagawa, K. Tomishige, *J. Phys. Chem. C* 116 (2012) 3079–3090.
- [54] F. Arena, G. Italiano, K. Barbera, S. Bordiga, G. Bonura, L. Spadaro, F. Frusteri, *Appl. Catal. A: Gen.* 350 (2008) 16–23.
- [55] S. Natesakhawat, J.W. Lekse, J.P. Baltrus, P.R. Ohodnicki, B.H. Howard, X. Deng, C. Matranga, *ACS Catal.* 2 (2012) 1667–1676.
- [56] A. Yin, X. Guo, W.L. Dai, K. Fan, *J. Phys. Chem. C* 113 (2009) 11003–11013.
- [57] K.L. Deutsch, B.H. Shanks, *J. Catal.* 285 (2012) 235–241.
- [58] A. Bienholz, H. Hofmann, P. Claus, *Appl. Catal. A: Gen.* 391 (2010) 153–157.
- [59] Y. Román-Leshkov, M. Moliner, J.A. Labinger, M.E. Davis, *Angew. Chem. Int. Ed.* 49 (2010) 8954–8957.
- [60] V. Choudhary, S.H. Mushrif, C. Ho, A. Anderko, V. Nikolakis, N.S. Marinkovic, A.I. Frenkel, S.I. Sandler, D.G. Vlachos, *J. Am. Chem. Soc.* 135 (2013) 3997–4006.
- [61] W.R. Gunther, Y. Wang, Y. Ji, V.K. Michaelis, S.T. Hunt, R.G. Griffin, Y. Román-Leshkov, *Nat. Commun.* 3 (2012) 1109.
- [62] Y. Kanie, K. Akiyama, M. Iwamoto, *Catal. Today* 178 (2011) 58–63.
- [63] S. Koso, Y. Nakagawa, K. Tomishige, *J. Catal.* 280 (2011) 221–229.
- [64] K. Chen, K. Mori, H. Watanabe, Y. Nakagawa, K. Tomishige, *J. Catal.* 294 (2012) 171–183.
- [65] Y. Amada, H. Watanabe, Y. Hirai, Y. Kajikawa, Y. Nakagawa, K. Tomishige, *ChemSusChem* 5 (2012) 1991–1999.
- [66] N. Ota, M. Tamura, Y. Nakagawa, K. Okumura, K. Tomishige, *Angew. Chem. Int. Ed.* 54 (2015) 1897–1900.
- [67] Y. Amada, N. Ota, M. Tamura, Y. Nakagawa, K. Tomishige, *ChemSusChem* 7 (2014) 2185–2192.